Raman spectra of hot-pressed boron suboxide

Ronald Machaka[1,2]*, Bonex W. Mwakikunga[3,4], Elayaperumal Manikandan[5], Trevor E. Derry[1,6], Iakovos Sigalas[1,2]

[1]*DST/NRF Centre of Excellence in Strong Materials, University of the Witwatersrand, Private Bag 3, Wits, Johannesburg 2050, South Africa*

[2]*School of Chemical and Metallurgical Engineering, University of the Witwatersrand, Private Bag 3, Wits, Johannesburg 2050, South Africa*

[3]*CSIR National Laser Centre, P.O. Box 395, Pretoria 0001, South Africa*

[4]*Department of Physics and Biochemical Sciences University of Malawi, The Polytechnic Private Bag 303, Chichiri, Blantyre 0003 Malawi*

[5]*CSIR National Centre for Nano-Structured Materials, P.O. Box 395, Pretoria 0001, South Africa*

[6]*School of Physics, University of the Witwatersrand, Private Bag 3, Wits, Johannesburg 2050, South Africa*

*Corresponding author. Tel: (+27) 11- 717- 7534; Fax: (+27) 11- 717- 6879; E-mail: ronald.machaka@wits.ac.za (R. Machaka).

Received: 24 Sept 2010, Revised: 8 Nov 2010 and Accepted: 15 Nov 2010

ABSTRACT

Despite hot pressing being the most popular method of consolidating B_6O powder, the Raman spectrum of polycrystalline hot-pressed B_6O was until now poorly understood. Yet, recent reports have contributed to the understanding of only high-pressure and high-temperature sintered B_6O. Using an automated method for subtraction of the fluorescence background from Raman measurements, the first- and second-order Raman spectra of B_6O and their dependence on the wavelength of the excitation line from a green Argon ion (Ar^+) laser are reported. Our results confirm the existence of observable highly resolved first- and second-order Raman modes measured at ambient conditions using a green Ar^+ ion laser as the source of excitation. We also extend our study to present a comparative analysis of our recovered first-order Raman spectra and previously reported first-order Raman spectra other α-rhombohedral boron type based ultra-hard boron-rich ceramic materials. The results show an overall good agreement. Copyright © 2011 VBRI press.

Keywords: Hot-pressed boron suboxide; B_6O; Raman spectroscopy; fluorescence background subtraction.

Ronald Machaka is a Ph.D candidate at the University of the Witwatersrand, in the School of Chemical and Metallurgical Engineering. Ronald obtained his M.Sc. by Research in Material Science Physics with merit from the University of the Witwatersrand. Ronald also holds a B.Sc. (Hons) in Applied Physics from the National University of Science and Technology, Zimbabwe. Ronald is affiliated to the DST/NRF Centre of Excellence in Strong Materials, Powder Metallurgy Association (SA), and the South African Institute of Physics. Current interests include boron-rich superhard ceramic composites, ion beam modifications, finite element modelling, Ni-base superalloys, and foot-bridges.

Bonex Wakufwa Mwakikunga is a Senior Lecturer in the Department of Physics and Biochemical Sciences at the Polytechnic of the University of Malawi. He obtained his PhD from the University of the Witwatersrand in 2009. He has taught and done research in environmental radioactivity and solid state physics. His interests in materials science led him to win many

scholarships and awards, including the Joint Japan/World Bank Graduate Scholarship Programme, enabling him to conduct research both at the University of the Witwatersrand and the Council for Scientific and Industrial Research (CSIR). At the CSIR he has worked in the National Centre for Nano-Structured Materials (NCNSM) and the National Laser Centre (NLC) where he is currently carrying out research on smart materials.

E. Manikandan is working as Senior Research Scientist at National Centre for Nano Structured Materials (NCNSM), Council for Scientific & Industrial Research (CSIR), Pretoria, SA. He is actively involved with the synthesis, characterization and functionalization of advanced industrials materials (AIM) for a variety of applications. He has keen interest on in-situ/online measurements (such as GIXRD, Raman Spectroscopy, FIB-Electron Microscopy) during (i) ion implantation, (ii) PLD growth of nanoparticles SW/MW-CNTs, oxide semiconductor multi-layer, metal/Si and metal/metal systems. Moreover, He has recently established

LIPS/LIBS technique (laser induced plasma/breakdown spectroscopy) for laser synthesis of single-wall CNTs and their growth mechanism.

akovos Sigalas is currently Element Six Professor of Ceramic Science at the University of the Witwatersrand. He is also Focus Area Coordinator (Ceramics Focus Area) in the DST/NRF Centre of Excellence in Strong Materials. He holds a PhD in experimental solid-state physics from the University of Manchester, U.K, a Diploma in Advanced Studies in Science also from the University of Manchester, U.K. and a BSc Physics (Honours) from Athens University, Greece. Prior to joining the University of the Witwatersrand, Prof Sigalas worked as lecturer at various Greek Universities (1975-1980), at CSIR, RSA (1980) and then at Element Six Pty Ltd as research manager (1991). He has 54 publications in international refereed journals, 25 patents, over 60 technical reports, and contributed to two books. His research interests include hard ceramic materials, suitable for cutting tool and wear part applications, nanostructured ceramics, and ceramics reinforced titanium metal.

Introduction

Boron has the second most complicated structural chemistry among all elements at ambient conditions after carbon. This is evident from the extremely large number of simple and complex compounds and structures that it can form and their wealth of interesting physical and chemical properties [1]. Among other fascinating compounds it can form is boron suboxide – B_6O, a boron-rich super-hard ceramic material characterised by an α-rhombohedral boron type structure (space group $R\bar{3}m$) [1–5] which is similar to those of boron carbide – B_4C [6, 7], aluminium magnesium boride – $AlMgB_{14}$ [8], and the newly synthesized boron subnitride – $B_{13}N_2$ [9, 10].

With hardness values reported between 24 GPa and 45 GPa [7, 11, 12], B_6O is sometimes considered to be the third hardest material only after diamond (~ 100 GPa) and cubic boron nitride (~ 60 GPa) [4, 13, 14]. In addition to the super-high hardness and low density, the ceramic material exhibits a rather unusual and wide range of superior properties that includes high mechanical strength, high chemical inertness, thermal stability, a high melting point, and good wear resistance [4, 15]. Furthermore, B_6O can be synthesized without the need for high pressures [4; 16] (hot-pressing is also an example, see [4, 14, 17]) unlike diamond or cubic boron nitride [15, 18]. This significantly augments to the commercial attractiveness of B_6O-based composites as potentially attractive candidates for high-wear applications where both abrasive resistance and thermal stability are required [15, 18, 19].

Raman spectroscopy is a valuable non-destructive technique universally used to characterize materials. A Raman spectrum often serves as a material fingerprint, with each peak in the spectrum corresponding to a unique vibrational mode of the lattice. In most typical laboratories, the green Argon ion (Ar^+) laser beam is the commonly used Raman excitation sources 514.5 nm.

Recently, Solozhenko *et al.* [20] reported that the first- and second-order Raman spectra of HPHT B_6O powders become observable when UV or IR wavelengths excitation beams are used. However, uniaxial hot pressing is the most cost-effective method of consolidating ceramic powders to full density ceramic compacts with controlled microstructures in a typical laboratory [18, 19]. A literature survey of the Raman response of polycrystalline hot-pressed B_6O shows very little has previously been reported on the characterization to understand the Raman spectrum of hot-pressed B_6O [21]; partly because B_6O is characterized by a relatively weak Raman signal and a strong inherent fluorescence background. In fact, some of the previously reported spectra are far from observable [20]. As a result, an understanding of the Raman spectra of uniaxially hot-pressed B_6O is a limited if not poor, especially when a green Ar^+ laser excitation source is used.

In this work, we attempt to investigate the local vibrational modes of hot-pressed B_6O using Raman spectroscopy using a green Ar^+ laser excitation source. We present a systematic investigation of this problem by means of deliberately (a.) using low-power excitation beams to minimize the heating and fluorescence effects on the sample surface, (b.) reducing the exposure duration, and (c.) the application of a suitable background subtraction on the measured Raman spectra. We report on the existence of observable first- and second-order Raman spectra of hot-pressed B_6O measured at ambient conditions using the green Ar^+ ion laser as the source of excitation.

We also extend the comparative study of the first-order Raman spectra of hot-pressed B_6O presented here to the other similar boron-rich based materials (α-rhombohedral boron, B_4C, and $B_{13}N_2$ to previously reported findings on this topic notably by Werheit and Filipov [22]) and Solozhenko *et al.* [9; 10] who all excluded hot-pressed B_6O in their comparison. The observed B_6O Raman-active modes are in close agreement with those theoretically calculated for boron-rich icosahedral compounds and strikingly similar to the other icosahedral boron-rich ultra-hard materials [10].

Experimental

Materials and Methods

Pure B_6O powder was prepared using a method described by Andrews *et al.* [11, 14] and Shabalala *et al.* [19]. The powders were uniaxially hot-pressed in hBN pots in argon gas environment at a temperature of 1800°C and a pressure of 50 MPa for 20 minutes. Hot-pressed samples were approximately 20 mm in diameter and 2 mm in thickness. The hot-pressed samples were sectioned to desired dimensions, mounted on Bakelite medium and then metallographically prepared to a 0.05 μm OPS finish for characterization by means of a unique combination of grinding and polishing.

The polished B_6O samples were analysed for phase composition using X-ray diffraction, with λ = 1.547 Å Cu K_α radiation. The powder diffraction patterns were collected using the Bragg-Brentano geometry over a 10° – 90° 2θ range in steps on 0.02° at a sampling time of

approximately 7 s per step and analysed. The voltage on the anode of the X-ray tube was 45 kV, and the current was 40 mA. The specimen's surface microstructure and composition were characterized by scanning electron microscopy (SEM) and energy-dispersive X-ray spectroscopy (EDX), respectively. A Philips XL30 environmental scanning electron microscope operating at 25 keV in backscattered secondary electron geometry was employed.

The micro-Raman spectroscopy measurements were performed in the back-scattering configuration at room temperature using a green 514.5 nm Ar$^+$ ion laser as the excitation source. An 1800 grooves/mm grating in the single spectrograph mode of a Jobin-Yvon T64000 Raman spectrometer was used. The measurements were performed using a 20 × Olympus objective and a ~ 1μm spot size diameter. The spectrum acquisition and pre-processing was done using the Horiba Jobin-Yvon LabSpec$^®$ 3.0 software package. An appropriate automated fluorescence suppression and background subtraction method was applied on the Raman scattering measurements. The scheme uses a series of linear extrapolations between adjacent minima within the spectrum. The laser power was deliberately kept low during all measurements to minimize the background fluorescence and possible temperature variation effects on the sample surface.

Results and discussion

Surface and compositional analysis

The surface morphology and compositional analysis of hot-pressed B_6O specimen as determined by SEM and EDX are shown in **Fig. 1**(**a**) and (**b**), respectively.

In general, the micrograph shows a homogeneous B_6O microstructure with visible pores on the specimen surface as a direct result of some considerable practical challenges in the densification of B_6O by hot pressing [**7, 17, 23**]. The analysis of the surface composition by EDX is also indicative of nominally pure B_6O phase. The observed iron contamination (< 1 wt. %) is expected and inevitable; it originates from abrasion of the steel ball and the containment cell during powder ball milling.

X-ray diffraction measurements

Fig. 2 shows the full profile X-ray powder diffraction pattern measured on the hot-pressed B_6O samples. As expected for B_6O material synthesized from amorphous boron, the pattern contains some broad amorphous peaks centred at the 2θ values 23.4° and 38° illustrated in **Fig. 2** inserts (**a**) and (**b**), respectively [**24**]. The broad amorphous peaks can be attributed to either to small amounts of starting amorphous boron or amorphous B_6O co-existing with crystalline B_6O [**19, 24**].
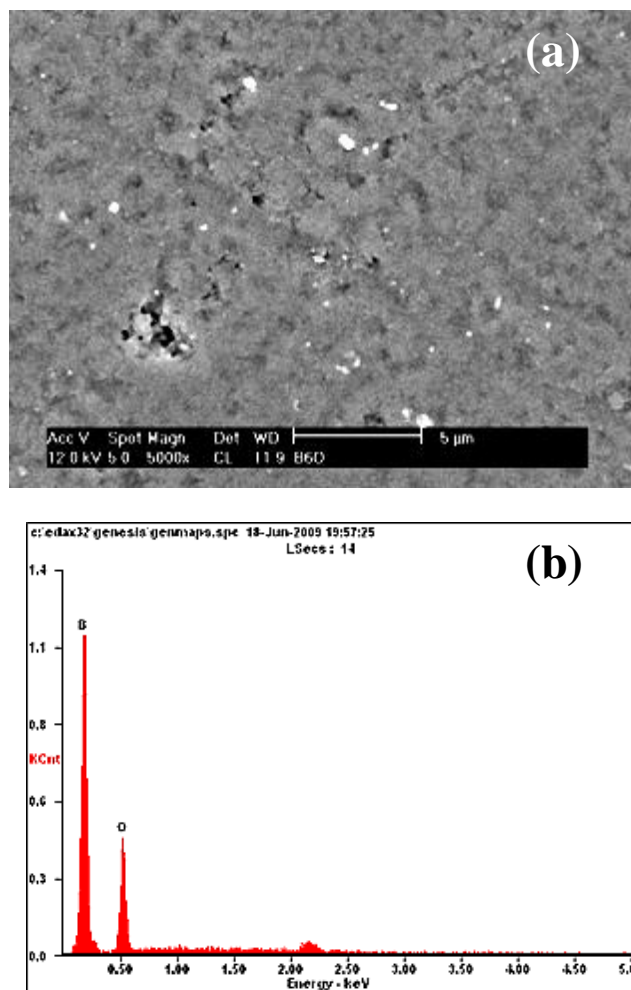

Fig. 1. Shows the SEM surface micrograph (a) and the EDX surface compositional analysis (b) of a hot pressed B_6O specimen. Iron contamination is responsible for EDX elemental peak observed around 2.25 keV.
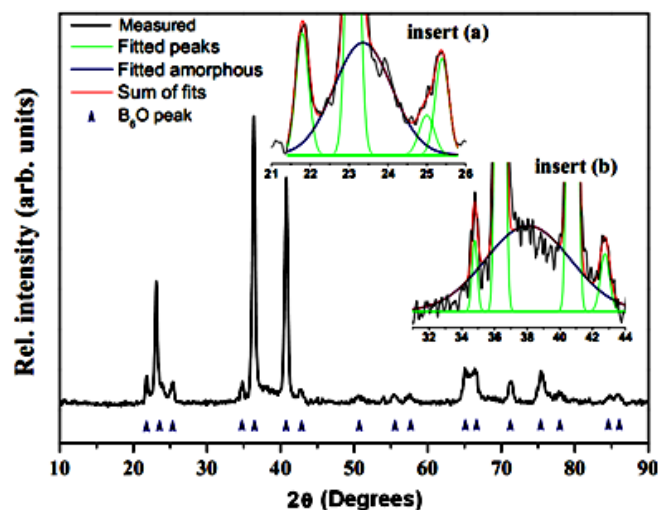

Fig. 2. The powder diffraction pattern of a sample of hot-pressed B_6O sample showing the predominance of the B_6O crystalline phase. Inserts (a) and (b) illustrate the broad amorphous peak fits.

The marked peaks in **Fig. 2** have been assigned to the α-rhombohedral boron structure (space group $R\bar{3}m$, JCPDS card number 31-210) consistent with the presence of a nominally pure polycrystalline B_6O phase [**19, 20, 25**]. An average crystallite size of 60 nm was determined using the conventional Scherrer method from the measured XRD pattern.

Raman scattering measurements

Boron has the second most complicated structural chemistry among all elements at ambient conditions after carbon. This is evident from the extremely large number of simple and complex phases and structures that it can form [**2, 26**]. In this work, Raman spectroscopy is a powerful analytical tool used here to investigate the local vibrational modes of the B_6O structure.

The experimentally measured and the fluorescence-background corrected Raman spectra of the uniaxially hot-pressed B_6O are shown on the same axis in **Fig. 3**. As expected [**20**], the experimentally measured Raman spectrum is weak and almost obscured in the presence of the inherent strong fluorescence background. The fluorescence-background corrected spectrum was obtained by means of the application of a fluorescence background suppression scheme, using the Horiba Jobin-Yvon LabSpec® 3.0 software.
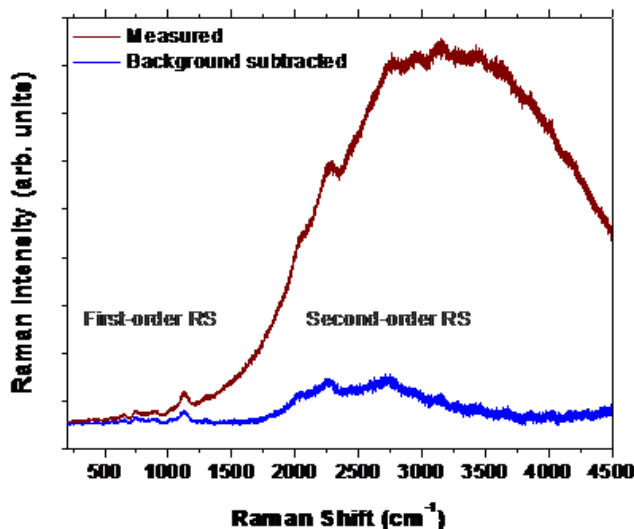

Fig. 3. The measured first- and second-order Raman spectra of B_6O and the fluorescence-background suppressed Raman spectra of B_6O.

The recovered the first-order, and second-order and tentatively the higher-order Raman spectra of B_6O are shown in **Fig. 4 (a)** and **(b)**, respectively. This demonstrates that even when the green 514.5 nm Ar^+ ion excitation laser is used, observable first- and second-order Raman spectra of B_6O can be observed. Simple precautions have to be taken, including: (a) deliberately using low-power excitation beams to minimize the heating and fluorescence effects on the sample surface, (b) reducing the exposure duration, and (c) the application of a suitable background subtraction scheme on the measured Raman spectra. **Table**

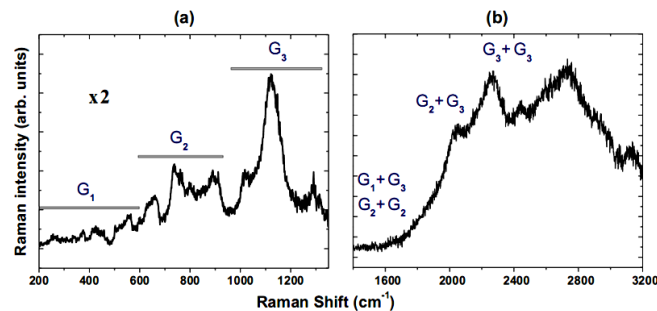**1** below gives a summary of the observed Raman peaks and the tentative peak position analysis.

Fig. 4. Shows the fluorescence-background corrected first- and second-order Raman spectra of B_6O, respectively. The second-order Raman modes are a combination of the first-order Raman active phonons.

We confirm that the peak positions are not affected by the subtraction scheme, but we acknowledge that the width could be slightly influenced.

For B_6O [**20, 27**], and other boron-rich solids that are based on the β-rhombohedral boron type crystal structure [**26, 22**], theoretical calculations predict twelve Raman active phonons modes, for an ideal $R\bar{3}m$ α-rhombohedral structure. However, for a real hot-pressed polycrystalline B_6O structure characterized with oxygen deficiency, intrinsic defects, and a slightly distorted β-rhombohedral boron type crystal structure Raman modes exceeding twelve are expected [**22, 27**].

For analysis, the first-order Raman spectra of B_6O has been sub-divided into three spectral band groups of the observed modes based on their positions (G_1, G_2, and G_3) as illustrated in **Fig. 4 (a)**. The G_1 band comprises vibrational modes observed below 600 cm^{-1}, G_2, modes between 600 cm^{-1} and 950 cm^{-1}, while G_3, comprises modes between 950 cm^{-1} and 1200 cm^{-1}. The assignment of individual peaks follows a similar approach to that reported by Solozhenko *et al.* [**20**]. **Table 1** summarises the observed Raman bands shown in **Fig.** 4 (a) and (**b**).

First-order groups of Raman modes

G_1 group of Raman modes: We have attributed the G_1 group of Raman peaks to vibrational modes involving the oxygen atom.

(a) When compared to the Raman spectra of HPHT synthesized B_4C, and $B_{13}N_2$ (illustrated in **Fig. 5** below), the G_1 Raman modes of the uniaxially hot-pressed B_6O material measured in this work are relatively weaker and broader.

(b) In particular, the Raman peak observed at 373 cm^{-1}, which is characteristic of the O–O chain vibration, is of very weak intensity and barely visible.

(c) The vibration at 425 cm^{-1} is attributed to the bending mode of the three-atomic chain.

(d) The relatively sharp feature at 500 cm^{-1} corresponds to the symmetric stretching of the B–O–B triatomic chain,

(e) The narrow line just above 500 cm^{-1}, has been attributed to the motion of the entire B$_{12}$ icosahedron about oxygen atom [20].

Table 1. Shows a summary of the measured Raman data and the peak assignments. The following notations evaluate the intensity qualitatively: s+s, sharp and strong; s+b, sharp but broad; s+w, sharp but weak; m, medium; w, weak; vw, very weak; b, broad.

Group	Peak Position (cm^{-1})		Band	Remarks
FIRST ORDER RAMAN MODES				
	259.6	b+w	π	Icosahedral chain (B-O) phonon
	373.4	w	B1	Vibrational motion of the (O-O) pair
	425.9	b+a	π	Bending vibration of the B-O-B chain
G$_1$	500.9	s+w	B2	Symmetrical stretching of the B-O-B chain
	555.5	m	B3	
	600.6	s+w	τ	Motion of the icosahedral boron atoms about O
	625.1	b	τ	
	736.9	s+s	B4	
G$_2$	762.8	sh	B5	Motion of the boron atoms in the icosahedra
	797.4	m	B6	
	891.9	m	B7	
	1016.4	m	B8	
G$_3$	1119.9	s+s	B10	The inter-icosahedral boron vibration
	1154.8	sh	B11	
	1288.2	m	B12	
SECOND-ORDER RAMAN MODES				
G$_1$+G$_3$	—	—	ψ	G$_1$ + G$_3$ two-phonon combinations
G$_2$+G$_2$	—	—	ψ	G$_2$ + G$_2$ two-phonon combinations
G$_2$+G$_3$	2022	s+s	B7+B10 B7+B11	
G$_3$+G$_3$	2230—2260	s+s	B10+B10 B10+B11 B11+B11	G$_2$ + G$_3$ two-phonon combinations
	2430.7	m	B12+B12	
HIGHER-ORDER RAMAN MODES				
	2723.6	s+b	π	
	2970.8	sh	π	
	3134.3	m	π	Observed but there is a lack of information
	3275.7	m	π	
	3256.4	w	π	

NOTES
π — observed but there is a lack of information
τ — assignment is speculative
ψ — expected but not observed

We have attributed the observations items (a) and (b) to the non-stoichiometric composition of the hot-pressed B$_6$O material. Following the conclusions of Olofsson and Lundstrom in ref. [24], oxygen atoms are situated at interstitial holes between icosahedra at non-bonding distances from each other. We also speculate here that the weak modes referred to in items (c– e) are relatively weak, this is indicative to the poor state of occupancy of the B–O–B chain linking the icosahedra.

Fig. 5 extends the comparison of the Raman spectra of boron-rich solids that are based on the α-rhombohedral boron type crystal structure made in reference [10], and references therein. Note that the B$_4$C, and B$_{13}$N$_2$ therein were synthesized under HPHT conditions and the B$_6$O, which is the subject of this study is a hot-pressed material. Compared with other icosahedral boron-rich solids, the Raman scattering of hot-pressed polycrystalline B$_6$O is extraordinarily weak.

G$_2$ and G$_3$ groups of Raman modes: It is generally accepted that all the lines observed between 600 and 1200 cm^{-1} are usually attributed to vibrations of the atoms of boron-rich B$_{12}$ icosahedra. The G$_2$ group of Raman modes observed between 600 and 1100 cm^{-1} correspond to the intra-icosahedral B–B bonds.
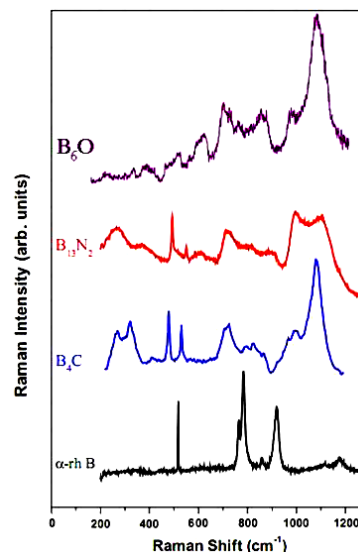

Fig. 5. A comparison of the Raman spectra of B$_6$O (our measurements, in purple) and other boron-rich based materials, B$_{13}$N$_2$, and B$_4$C. Note: The B$_4$C and B$_{13}$N$_2$ materials were synthesized under HPHT conditions. Diagram adapted from ref. [10] and all the measurements were measured at room temperature.

The G$_3$ group of Raman modes were observed between 950 and 1200 cm^{-1} and these correspond to the inter-icosahedral modes.

(i) We observe that at higher Raman shift frequencies, structural disorder is likely to be responsible for most of the observed broadening [28].

(ii) In addition to broadening, both the G$_2$ and G$_3$ bands of the Raman peaks appear to be riding on two strong, broad but distinct peaks (800 and 1160 cm^{-1}), respectively, which corresponds to amorphous and β-rhombohedral boron [22] – observation is consistent with the XRD pattern observed in **Fig. 2**.

(iii) Since the distances of B$_{12}$ icosahedral boron atoms are nearly the same in B$_6$O, B$_4$C and B$_{13}$N$_2$, we expect their respective G$_2$ and G$_3$ bands to be closely related. From **Fig. 5**: notably the strong phonon of B$_4$C at 1430 cm^{-1} due to the stretching mode of the three-atomic chain [10] is missing in the spectrum of B$_6$O.

(iv) However, the highest first order mode of 1288 cm^{-1} is observed in the spectrum of B$_6$O but is not reported in the spectrum of B$_4$C.

(v) The strong phonon of B$_6$O at 1288 cm^{-1} is attributed to intericosahedral phonons like in α-rhombohedral boron [20].

Second- and higher-order groups of Raman modes

Fig. 4(b) shows measured Raman bands above 1500 cm^{-1}, the second-order Raman spectra of B$_6$O. The origins of these bands may be due to the two-phonon combinations of the modes from the G$_1$, G$_2$ and G$_3$ groups of Raman bands [20]. The notable absence of the G$_1$ + G$_3$ and G$_2$ + G$_2$ combinations is easy to see given the relatively weaker G$_1$ phonon modes observed. Subsequently, it is therefore tentatively attributed to the non-stoichiometric composition

of the hot-pressed B_6O material. In **Table 1**, we satisfactorily summarize all observed second-order Raman modes by considering combination of the first-order Raman active phonons with good agreement. If the 1288 cm^{-1} mode is considered as a first-order Raman mode, we can speculate that the medium-sized 2430 cm^{-1} peak would also be easily considered as second-order as well [**20**].

The weak Raman features observed beyond 2430 cm^{-1} clearly do not appear to follow the same phonon-phonon linear combination rule as the second-order Raman modes. However, although these higher-order Raman bands have well-defined frequencies and widths their nature and origins is less clear to us at present. Probably because they are inherently weak and the number of possible phonon-phonon mode combinations remarkably rises [**10**], simultaneously.

Conclusion

Based on the Raman scattering studies of hot-pressed B_6O we conducted using the 514.5 nm Ar^+ excitation, we conclude that as previously reported in [**20, 21**], we observed that the Raman spectrum of hot-pressed B_6O is characterized by a relatively weak Raman signal and a strong inherent fluorescence background. However, contrary to some reports that the Raman spectrum of hot-pressed B_6O is unobservable when the 514.5 nm Ar^+ excitation source is used for the Raman scattering studies, our results confirm the existence of observable highly resolved first-, second- and higher-order Raman spectra. The measured Raman spectrum of hot-pressed B_6O is comparable to the Raman spectra of HPHT synthesized $B_{13}N_2$ and B_4C materials measured at ambient conditions using the same excitation source. For analysis, the first-order Raman spectrum of B_6O has been conventionally divided into three spectral band groups of the observed vibrational modes. The G_1 band comprises vibrational modes observed below 600 cm^{-1}, G_2, modes between 600 cm^{-1} and 950 cm^{-1}, while G_3, comprises modes between 950 cm^{-1} and 1200 cm^{-1}. The G_1 Raman modes of hot-pressed B_6O measured are relatively weak and sometimes barely visible; we have tentatively attributed the poor oxygen occupancy in the B–O–B chain linking the icosahedra. When compared to the Raman spectra of $B_{13}N_2$ and B_4C measured at ambient conditions using the same excitation source, the G_2 and G_3 Raman modes of hot-pressed B_6O are generally similar in characteristics. The general broadening of the G_2 and G_3 modes is consistent with fact that the B_{12} icosahedra are slightly distorted. The second- and higher-order Raman spectra are also observable; the origin of the second-order Raman modes has been attributed to the two-phonon combinations of the first-order vibrations (as illustrated in **Table 1** above). However, the nature and the origins of the higher-order Raman spectrum is less clear at present and required further investigations.

References

1. Albert, B.; Hillebrecht, H. *Angew. Chem. Int. Edit.* **2009**, *48*, 1521. **DOI:** 10.1002/anie.200903246

2. Lowther, J.E. *Physica B* **2002**, *322*, 173. **DOI:** 10.1016/S0921-4526(02)01180-8

3. Shirai, K. *J. Superhard Mater.* **2010**, *32*, 205. **DOI:** 10.3103/S1063457610030068

4. McMillan, P.F.; Hubert, H.; Chizmeshya, A.; Petuskey, W.T.; Garvie, L.A.J.; Devouard, B. *J. Solid State Chem.* **1999**, *147*, 281. **DOI:** 10.1006/jssc.1999.8272

5. Hubert, H.; Devouard, B.; Garvie, L.A.J.; O'Keeffe, M.; Buseck, P.R.; Petuskey, W. T.; McMillan, P.F. *Nature* **1998**, *391*, 376. **DOI:** 10.1038/34885

6. Suri, A.K.; Subramanian, C.; Sonber, J.K.; Murphy, T.S.R.Ch. *Int. Mater. Rev.* **2010**, *55*, 4. **DOI:** 10.1179/095066009X12506721665211

7. Herrmann, M.; Raethel, J.; Bales, A.; Sempf, K.; Sigalas, I.; Hoehn, M. *J. Euro. Ceram. Soc.* **2009**, *29*, 2611. **DOI:** 10.1016/j.jeurceramsoc.2009.03.002

8. Roberts, D.J.; Zhao, J.; Munir, Z.A. *Int. J. Refract. Met. H.* **2009**, *27*, 556. **DOI:** 10.1016/j.ijrmhm.2008.07.009

9. Kurakevych, O.O.; Solozhenko, V.L. *Solid State Commun.* **2009**, *149*, 2169. **DOI:** 10.1016/j.ssc.2009.09.019

10. Solozhenko, V.L.; Kurakevych, O.O. *JPCS* **2008**, *121*, 62001. **DOI:** 10.1088/1742-6596/121/6/062001

11. Andrews, A.; Sigalas, I.; Herrmann, M. WIPO Patent No. WO/2008/132675 **2008**.

12. Davies, G.J.; Sigalas, I.; Herrmann, M.; Shabalala, T.C. WIPO Patent No. WO/2007/029102 **2007**.

13. Chen, C.; He, D.; Kou, Z.; Peng, F.; Yao, L.; Yu, R.; Bi, Y. *Adv. Mater.* **2007**, *19*, 4288. **DOI:** 10.1002/adma.200700836

14. Andrews, A.; Herrmann, M.; Shabalala, T.C.; Sigalas, I. *J. Euro. Ceram. Soc.* **2008**, *28*, 1613. **DOI:** 10.1016/j.jeurceramsoc.2007.10.011

15. Itoh, H. *J. Ceram. Soc. Jpn.* **2004**, *112*, 121. **DOI:** 10.2109/jcersj.112.121

16. Jiao, X.; Jin, H.; Liu, F.; Ding, Z.; Yang, B.; Lu, F.; Zhao, X.; Liu, X. *J. Solid State Chem.*, **2010**, 183,1697 **DOI:** 10.1016/j.jssc.2010.05.031

17. Johnson, O.T.; Sigalas, I.; Ogunmuyiwa, E.N.; Kleebe, H.J.; Muller, M.M.; Herrmann, M. *Ceram. Int.* **2010**, *36*, 1767. **DOI:** 10.1016/j.ceramint.2010.02.035

18. Johnson, O.T.; Sigalas, I.; Herrmann, M. *Ceram. Int.* **2010**, *36*, 2401. **DOI:** 10.1016/j.ceramint.2010.07.018

19. Shabalala, T.C.; McLachlan, D.S.; Sigalas, I.; Herrmann, M. *Ceram. Int.*, **2008**, *34*, 1713 **DOI:** 10.1016/j.ceramint.2007.05.010

20. Solozhenko, V.L.; Kurakevych, O.O.; Bouvier, P. *J. Raman Spectrosc.* **2009**, *40*, 1078. **DOI:** 10.1002/jrs.2243

21. Werheit, H.; Kuhlmann, U. *J. Solid State Chem.* **1997**, *133*, 260. **DOI:** 10.1006/jssc.1997.7452

22. Werheit, H.; Filipov, V. *In Raman Effect in Boron Rich Solids*, Orlovskaya, N.; Lugovy, M. (Eds.), Springer Netherlands, **2011**, pp. 29-43.

    DOI: 10.1007/978-90-481-9818-4_3

23. Herrmann, M.; Kleebe, H.J.; Raethel, J.; Sempf, K.; Lauterbach, S.; Muller, M.M.; Sigalas, I. *J. Am. Ceram. Soc.* **2009**, *92*, 2368.

    DOI: 10.1111/j.1551-2916.2009.03197.x

24. Olofsson, M.; Lundstrom, T. *J. Alloy Comp.* **1997**, *257*, 91.

    DOI: 10.1016/s0925-8388(97)00008-x

25. Itoh, H.; Yamamoto, R.; Iwahara, H. *J. Am. Ceram. Soc.* **2000**, *83*, 501.
    DOI: 10.1111/j.1151-2916.2000.tb01224.x

26. Werheit, H. *In Electric Refractory Materials;* Kumashiro, Y., Ed.; Marcel Dekker Inc., **2000**, pp. 589-654.

    DOI: 10.1201/9780203908181

27. Wang, Z.; Zhao, Y.; Lazor, P.; Annersten, H.; Saxena, S. K. *Appl. Phys. Lett.* **2005**, *86*, 041911.
    DOI: 10.1063/1.1857091

28. Lazzari, R.; Vast, N.; Besson, J. M.; Baroni, S.; dal Corso, A. *Phys. Rev. Lett.*, **1999**, *83*, 3230.
    DOI: 10.1103/PhysRevLett.83.3230